Yan, Shibo and Zeng, Xuesen and Brown, Louise and Long, Andrew (2017) Geometric modeling of 3D woven preforms in composite T-joints. Textile Research Journal . 004051751771209. ISSN 0040-5175

Geometric modelling of 3D woven preforms in composite T-joints

Journal:	*Textile Research Journal*
Manuscript ID	TRJ-17-0023.R1
Manuscript Type:	Original Manuscript
Keywords:	weaving < Fabrication, Fabrication < Fabrication, processing < Fabrication, composites < Materials
Abstract:	A common method to fabricate net-shaped 3D woven preforms for composite T-joints is to weave flat 3D preforms via a standard weaving machine with variation in binder yarn path and then separate the preform in the form of a bifurcation. Folding introduces fibre architecture deformation at the 3D woven bifurcation area. In this paper, a geometric modelling approach is proposed to represent the realistic fibre architecture, as a preprocessor for finite element analyses to predict composite structural performance. Supported by x-ray micro-computed tomography (μCT), three important deformation mechanisms are observed including yarn stack shifting, cross-section bending and cross-section flattening resulting from the folding process. Furthermore, a set of mathematical formulae for simulation of the deformations in the junction region are developed and satisfactory agreement is observed when compared with μCT scan results.

Nomenclature

Field Code Changed
Field Code Changed
Field Code Changed

H_{warp} - height of warp yarn

H_{weft} - height of weft yarn

W_{warp} - width of warp yarn

W_{weft} - width of weft yarn

D_{weft} - spacing of weft yarns between through-thickness layers

D_{warp} – spacing of warp yarn in the same layer

$\overline{R_n^{warp}}$ - radius of curvature of centreline of warp yarn cross-section on yarn layer n(μCT measurement)

$\overline{R_n^{weft}}$ - radius of curvature of centreline of weft yarn layer n(μCT measurement)

R_n^{warp} - radius of curvature of centreline of warp yarn cross-section on yarn layer n(calculated)

R_n^{weft} - radius of curvature of centreline of weft yarn layer n(calculated)

R_m – radius of compaction mould fillet

G_d - maximum width of the cross-sectional gap in a flattened weft yarn

S_θ - warp yarn angle shit

S_d - warp yarn displacement shit

d_o - offset distance from the centre of nearest unbent weft yarn

d - distance from a specific fibre layer within the yarn to the reference fibre layer

d_{max} - the maximum value of d

L_d - arc length difference between fibre on a specific fibre layer, distance d away from reference fibre layer, and fibre on reference layer

R_0 - radius of curvature of the reference fibre within a bent yarn

R_d - radius of curvature of the fibre that is distance d away from the reference fibre within a bent yarn

α - a proportion of arc length difference L_d

$\bar{\alpha}$ - the values of α for the ideally migrated fibres

L_{ABCD} - the arc length of fibre ABCD

l_0 - length of yarn width transition

w - displacement of out-of-plane fibre migration

w_k displacement of out-of-plane migration for fibre on fibre layer k within a yarn

$\overline{AB}$ - length of line AB

$\widehat{AB}$ - length of arc AB

$Area_{ext}$ - total fibre area in yarn extension

d_f - fibre diameter

n_f - the number of total fibre layers along the yarn height direction before flattening

W_{weft}^{ext} - weft yarn width extension

H_{weft}^{fla} - flattened height of weft yarn

W_{weft}^{fla} - flattened width of weft yarn

Introduction

3D woven composites are reinforced by 3D woven preforms containing yarns in x, y and z directions. 3D woven preforms, specifically for composite applications, are generally classified into orthogonal, through-the-thickness angle interlock and layer-to-layer angle interlock patterns. Design and manufacturing of emerging multi-axis 3D woven preforms incorporating bias yarn layers has also been proposed but the development is still at an early stage for applications.[1] 3D woven composites have drawn great attention in recent decades for their advantages such as higher through-thickness properties that can help to overcome the problem of delamination encountered by 2D laminates.[1] The exploration of 3D reinforced composites has been also extended to load-bearing profiles like T, I, and Pi shaped joints. There are three basic ways to manufacture 3D reinforced composite joints with woven preforms. The first method is to use 2D woven fabric lay-ups, reinforcing the through-thickness direction with stitching or Z-pinning.[2,3] The second way is to weave flat 3D preforms via a standard weaving machine with variation of binder yarn path to form locally unreinforced planes (bifurcations) and then fold the preforms into the desired shape.[4-7] The third

Formatted: Font color: Red

way is to fabricate the preform directly into a complex 3D shape through a specially developed 3D weaving loom.[8-10] Although composites reinforced by the first method can offer better damage tolerance in terms of delamination than 2D laminated joints subjected to equivalent loads,[2,11] they can be less competitive in in-plane properties because of geometric defects or fibre damage caused by retrospectively inserting through-thickness reinforcements.[12] In addition, due to the high investment and innovation needed for developing a special 3D loom for the third kind of preform, 3D preforms woven by a conventional loom are popular for current composite T-joints.

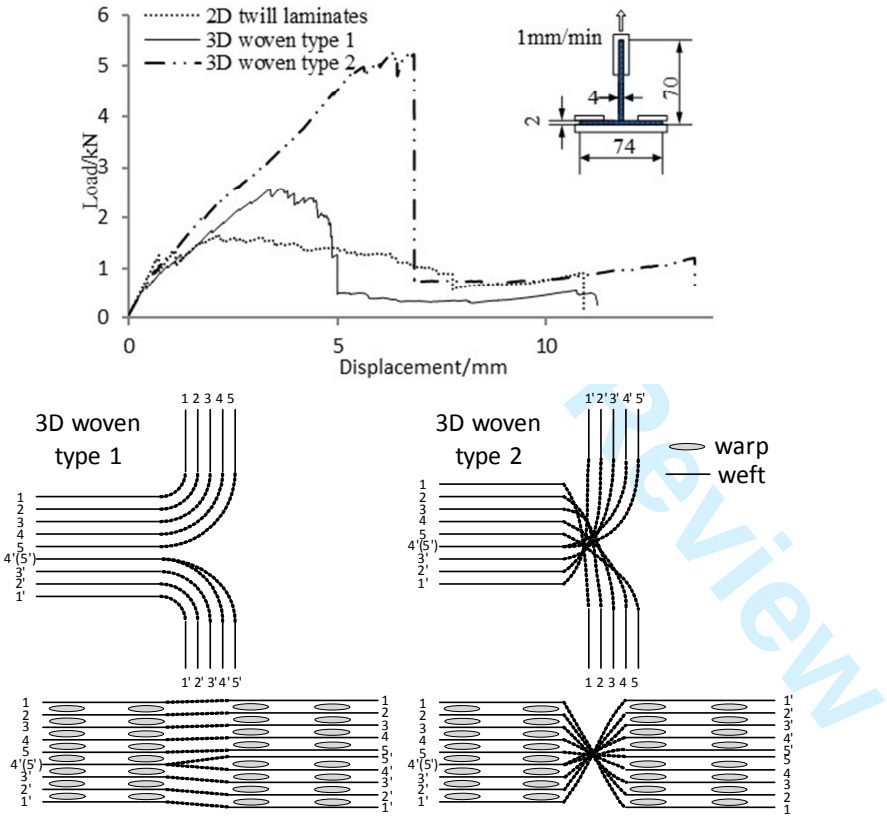

Figure 1. Top, load-displacement curves for the two types of 3D woven composite T-joints in comparison with an equivalent 2D twill woven T-joint[16]; bottom, schematic woven structures for the T-joints showing weave variation ~~in the noodle region~~at the junction (dashed line area), with binders omitted

Formatted: Font: 10 pt, Font color: Red

However, deformation is likely to occur when folding a flat woven preform into a 3D shape. Because the internal architecture of a woven preform is complex, its variability in geometry can directly affect material properties such as permeability and formability.[13,14] At the micro-scale, the fibre misalignment in fibre

bundles was also found to have an influence on many aspects of composite behaviour.[15] Previous studies have also shown that reinforcement geometry plays an important role in determining the composite's mechanical properties, as two types of 3D woven composite T-joints with only weave variation at the 3D woven bifurcation area (in which the formed resin pocket is usually referred to as the 'noodle') were tested under the same tensile loading case but very different load-displacement responses were observed (Figure.1).[16] Thus, in order to closely predict the properties of composite T-joints reinforced by a flat woven 3D preform, it is necessary to model the fibre architecture as realistically as possible.

Characterising the realistic fibre architecture of 3D woven composites is difficult because of the complexity of the internal geometry, but this can benefit from the use of x-ray micro-Computer Tomography (μCT).[17,18] Some general frameworks for geometric modelling of woven preforms with respect to characterisation of yarn path, crimp and cross-section shape have been provided in the literature.[19-22] Furthermore, compaction induced yarn crimp and cross-section shape change were studied with a number of models,[23,24] however, as they are based on beam theory, numerically solved by the finite element method, they are computationally intensive. Some mathematical methods were also proposed to model yarn cross-section shape under compression. An energy based method used to characterise yarn deformation in compression was developed by Lomov and Verpoest[25] but the method asks for a measurement of the mechanical properties of yarns in bending and compression. Chen et.al[26,27] modelled yarn cross-section deformation of both single and multi-layer woven preforms under compaction at the mesoscopic level based on the assumption that yarn width deformation is negligible compared with the deformation of yarn thickness. The model is not applicable when yarn width change is significant, for instance for a yarn subjected to bending load. Cornelissen and Akkerman[28] observed yarn cross-section flattening in a cantilever experiment of yarns bending under their own weight. They concluded that cross-section flattening would affect the yarn flexural rigidity by one order of magnitude but they were not able to derive a trend from the experiment. However, yarn cross-section deformation in bending is significant as observed in this study via μCT analysis and an effective model is needed to capture this feature.

This paper focuses on the geometric modelling of 3D woven preform deformation caused by folding a flat woven preform into a T-piece, which is a typical fabrication process for composite T-joints. Through the μCT analysis of a compacted preform, three important deformation mechanisms specifically for this type of

preform were observed, namely yarn stack shifting, cross-section bending and cross-section flattening resulting from the folding process. These features have been geometrically modelled and the models have been validated against μCT analysis data of a 3D woven T-joint preform.

Material characterisation

The example preform reinforcing the composite T-joints is a 3D orthogonal weave provided by Sigmatex, UK based on Hexcel IM7 12K carbon fibre, which is woven flat on a Jacquard machine and folded into a T shape. 3D orthogonal weaves are 3D structures containing straight warp and weft yarns in the *x*, *y* directions and binders (also called 'warp weavers') that interlace with other yarns, at times, orientated in the through-thickness direction, providing high stiffness under tensile loading due to low yarn waviness.[10] The preform consists of 8 layers of warp yarns and 9 layers of weft yarns in the web, and 4 layers of warp yarns and 5 layers of weft yarns in the flange. A schematic woven structure for this preform before and after bifurcation is shown as '3D woven type 1' in Figure 1.

To characterize the intrinsic geometric features of this type of preform for composite T-joints, the dry preform was compacted into a T-shape acrylic fixture and analysed via μCT as shown in Figure 2. The web section of the preform was firstly fitted in the fixture before bifurcation of the flange section, thus no deformation in the web is likely to be expected from preform bifurcation and the part of the preform contacting the fixture corner would conform to its radius of curvature. The GE phoenix v|tome|x m machine used a current of 240 μA and a voltage of 120 kV to achieve the imaging resolution of 30 μm per pixel in scanning. The compaction leads to an average fibre volume fraction of 45% which is calculated based on the preform areal weight with 4mm thickness in the web and 2mm in the flange. The preform has two geometric changes in its left-hand side: one is that the warp yarns at the junction (curved region) are in twice the filament count as those in the web; the other is a weft layer in the web (numbered as 4'(5') in Figure 2) is formed of twofold weft yarns as used in other layers and separated into two layers (layer 4' and 5') at the flange, for the purpose of yarn layer balance in the flange. Meanwhile, the flange part of the preform was woven with warp yarns of 24k filament count.

Formatted: Font color: Red

Formatted: Font color: Red

Formatted: Font color: Red

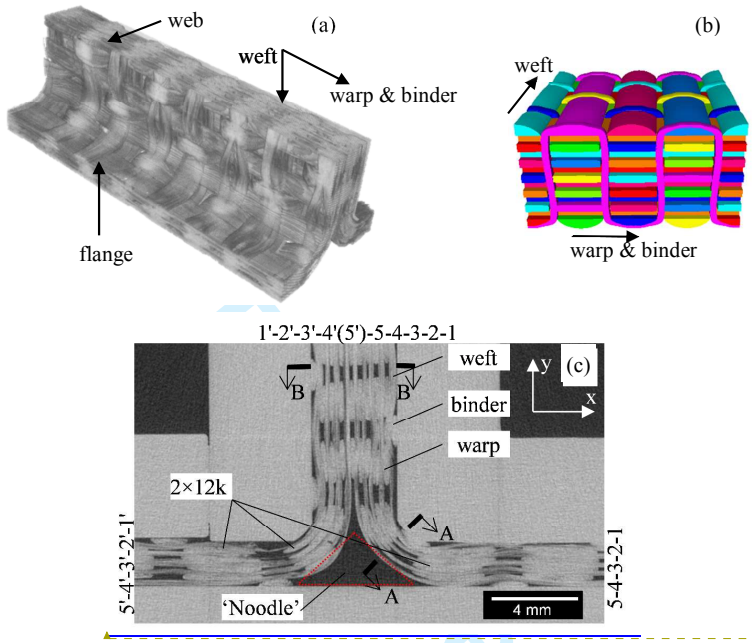

Figure 2. µCT scan of the preform: (a) preform visualised via volume rendering from µCT showing the yarn directions; (b) schematic 3D orthogonal weave pattern (created by TexGen) ; (c) µCT section view of the preform with the numbers showing the numbering of weft layers

In order to validate the proposed geometric modelling approach, necessary geometric parameters measured from the preform are listed in Table 1. In addition, the intra-yarn fibre volume fractions at different locations inferred from the cross-sectional data were given, assuming a rectangular cross-section for the yarns. Measurements of each parameter were made using the software ImageJ at a number of µCT slices covering different yarns, from which the average and standard deviation (SD) were obtained. The folding process introduces additional yarn deformation at the junction, and three significant features were observed as described in the following sections.

Table 1. Measured geometric parameters of the 3D woven preform through µCT

Location	Yarn	Height(SD) in mm	Width(SD) in mm	Intra-yarn fibre volume fraction	Number of measurements
Web	warp(surface[1])	0.32(±0.04)	1.72(±0.08)	46.30%	20
	warp(internal[2])	0.29(±0.02)	1.97(±0.08)	44.61%	50
	weft(surface)	0.35(±0.03)	1.71(±0.07)	40.22%	20
	weft(internal)	0.32(±0.03)	2.00(±0.13)	39.82%	50

Formatted: Font:

Web crossover[3]	warp(surface)	0.22(±0.04)	1.81(±0.08)	64.00%	20
	warp(internal)	0.17(±0.02)	2.02(±0.12)	74.21%	20
	weft(surface)	0.30(±0.04)	1.65(±0.12)	51.48%	20
	weft(internal)	0.19(±0.04)	1.87(±0.09)	71.73%	20
Flange	warp(surface)	0.35(±0.04)	3.61(±0.14)	40.34%	20
	warp(internal)	0.31(±0.03)	3.85(±0.08)	42.71%	20
Section A-A	weft layer1	0.28(±0.01)	2.63(±0.08)	34.61%	20
	weft layer2	0.29(±0.03)	3.01(±0.11)	29.20%	20
	weft layer5	0.29(±0.02)	3.57(±0.04)	24.62%	20
		Spacing in the same layer (mm) 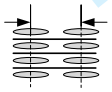	Spacing between through-thickness layers(mm) 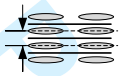		
	warp	2.71(±0.03)	0.45(±0.10)		20
	weft	3.33(±0.16)	0.44(±0.04)		20

[1] surface yarns are those on the layers next to compaction fixture surfaces
[2] internal yarns are all other yarns except surface yarns
[3] crossover refers to the locations where warp and weft yarns intersect

Warp yarn shift

The first distinctive deformation is the shift of the warp yarn stack ~~in the noodle region~~at the junction, in the direction orthogonal to the yarn length direction. The warp yarns within the same stack are aligned vertically with each other before folding the preform, but their relative position is shifted after folding due to the rigid body transformation ~~in the noodle region~~at the junction. However, the warp yarn shift could be suppressed by the surrounding binder yarns.

Formatted: Font color: Red

Formatted: Font color: Red

The shift begins in the warp yarn stack at the bend as marked in Figure 3, and is followed by the next 1-2 stacks in the flange. It is noted from the μCT scan that this phenomenon is most evident in the noodle area, and the level of shift reduces in the following stacks of warp yarns in the flange. To quantify the shift of the warp yarn stack, shift in the bend can be represented by angle shift S_θ, which is measured as the angle between the two lines connecting centres of yarns to the normal direction of each yarn. Shift of the

following stack is depicted as displacement shift S_d representing the horizontal distance between two yarn centres as illustrated in Figure 3.

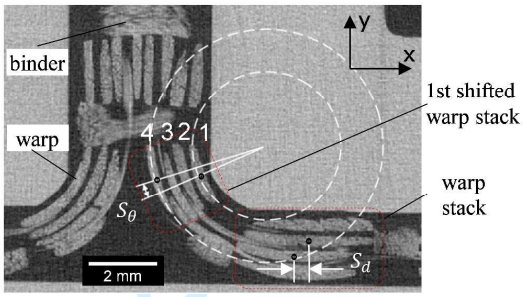

Figure 3. Warp yarn shift quantification ~~in the noodle region~~at the junction (weft yarns not shown); numbers show the numbering of warp layers

Formatted: Font: 10 pt, Font color: Red

Warp yarn cross-section bending

Bent cross-sections of warp yarns were observed ~~in the noodle region~~at the junction. As shown in Figure 3, each warp yarn bends about the centreline (or centre-plane) of its cross-section uniformly along its length direction and its shape complies with the curvature of the adjacent weft yarn layers. For this 90° folded preform, the centreline of each weft layer in the bend follows the path of a quarter of the circumference of a circle. As a result, the centrelines of bent warp yarn cross-sections could be approximated with circular paths of different radii. The measured radii of curvature of centrelines of bent warp cross-sections (R_n^{warp} in Figure 6) and weft yarn layers (R_n^{weft} in Figure 5) are listed in Table 2.

Formatted: Font color: Red

Table 2. Measured and calculated radii of curvature of centrelines of bent warp yarn cross-sections and weft yarn layers, here subscript *n* is the yarn layer number (mm; 5 measurements)

	Measured values		Calculated values (Eq.(1))	
	$\overline{R_n^{weft}}$	$\overline{R_n^{warp}}$	R_n^{weft}	R_n^{warp}
Layer 1	2.19(±0.07)	2.38(±0.10)	2.18	2.4
Layer 2	2.42(±0.12)	2.78(±0.15)	2.62	2.84
Layer 3	3.11(±0.08)	3.11(±0.14)	3.06	3.28
Layer 4	3.63(±0.12)	3.71(±0.13)	3.5	3.72
Layer 5	4.25(±0.10)		3.94	

Weft yarn cross-section flattening

In Figure 4, section view A-A of Figure 2 shows the cross-sections of weft yarns at the middle of the bend arc, while section B-B denotes cross-sections of weft yarns in the flat region. It is obvious that the cross-sections of weft yarns at section A-A are significantly flattened, i.e. an increase in yarn width and decease in yarn height, especially for those not sitting in the peak or trough of the binder yarn path since here yarn flattening is not constrained by binders. The cross-section data of flattened weft yarns without binder constraint at position A-A were measured from the μCT scan and results are listed in Table 1. The layer sequence of weft yarns in section A-A is numbered as Figure 2 shows. From further observation of μCT images, the most slender cross-section of weft yarn occurs at position A-A in Figure 2, from where it transitions symmetrically back to the dimension of the yarn cross-section in the flat part of the preform. It is also observed that the length of yarn width transition varies for yarns on different layers, but all the flattened yarns are of almost same height as shown in Table 1.

Meanwhile, a number of gaps in yarn cross-sections at section A-A were observed, which caused serrated cross-section shapes in most of the weft yarns as marked in Figure 4. A number of different slices near section A-A indicate this phenomenon and therefore it is unlikely to be an artefact of the μCT scan. The position of each gap appears random as observed and the cross-sectional gap is simply quantified by its maximum width that is named gap distance G_d. The value of G_d is no more than 1.5mm from several measurements. The flattening and cross-sectional gaps of weft yarns at the bend partly result from fibre migration when the preform is folded.[15]

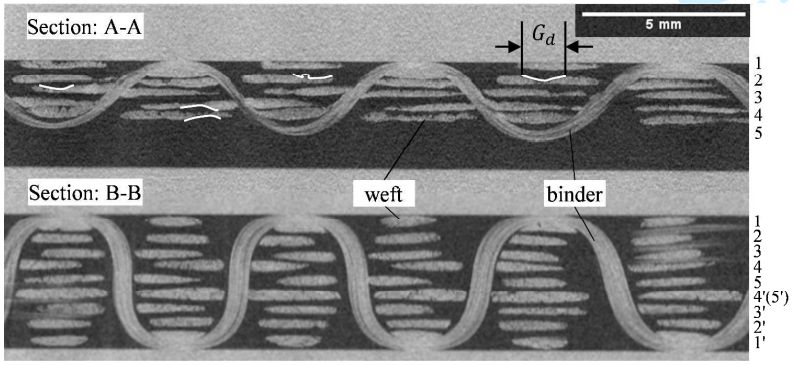

Figure 4. μCT images showing weft yarn flattening (A-A: flattened; B-B: non-flattened); serrated cross-section shapes are marked in Section A-A

Geometric modelling

Warp yarn shifting

The warp yarn shift is inevitable due to the rigid body transformation ~~in the noodle region~~at the junction. Each warp yarn has a different radius of curvature of cross-sectional centreline to the fillet origin O. As illustrated in Figure 5, half of a flat piece of 3D woven preform (left) is folded to a 90° angle (right). R_1^{weft}, R_2^{weft} and R_3^{weft} are the radii of curvature of centrelines for weft yarns on layer 1, 2 and 3 respectively. As the radius of the inner surface of a T-piece is confined by the mould corner radius R_m, the following can be obtained:

$$\begin{aligned} R_1^{weft} &= R_m + \frac{H_{weft}}{2} \\ R_2^{weft} &= R_1^{weft} + D_{weft} \\ R_3^{weft} &= R_2^{weft} + D_{weft} \\ R_n^{warp} &= (R_n^{weft} + R_{n+1}^{weft}) / 2 \end{aligned} \quad (1)$$

where H_{weft} is the height of the weft yarn; D_{weft} is the spacing between through-thickness weft layers; R_n^{warp} is the radius of curvature of centreline for the warp yarn cross-section on layer n.

Assuming there is no yarn sliding, angle shit S_θ between warp yarn layer 1 and layer 2 (in radians) in Figure 5 can be expressed as:

$$S_\theta = \frac{2(D_{warp} - d_o)}{R_1^{weft} + R_2^{weft}} - \frac{2(D_{warp} - d_o)}{R_2^{weft} + R_3^{weft}} = (D_{warp} - d_o)\left(\frac{1}{R_1^{warp}} - \frac{1}{R_2^{warp}}\right) \quad (2)$$

where D_{warp} is the warp yarn spacing within the same layer, and d_o the offset distance from the centre of nearest unbent weft yarn describing the position where the weft yarns start to bend; therefore $D_{warp} - d_o$ denotes the arc length in between bending onset position and bent yarn centre along the bend.

Formatted: Font color: Red

Field Code Changed

Field Code Changed

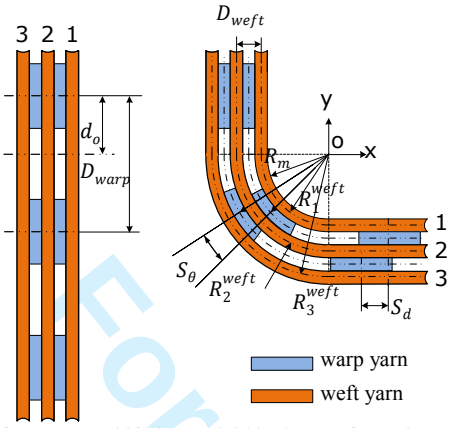

Figure 5. Schematic view of warp yarn shift due to rigid body transformation

Also, the displacement shift S_d in adjacent layers for the following stacks of weft yarns can be described as:

$$S_d = \frac{\pi}{2}\left(\frac{R_2^{weft} + R_3^{weft}}{2} - \frac{R_1^{weft} + R_2^{weft}}{2}\right) = \frac{\pi}{2} D_{weft} \quad (3)$$

Field Code Changed

Warp yarn cross-section bending

Yarn cross-section shapes have been approximated by a number of researchers by elliptical, power elliptical and lenticular shapes which can be defined by parametric equations in two dimensions.[19] Therefore it is convenient to model the cross-section deformation by a parameterized transformation that can apply to every current parametric cross-section shape rather than defining a new description for a curved cross-section. The cross-section of one warp yarn is presented in Figure 6 prior to and after deformation, where x and y represent the original yarn width and yarn height directions, and the origin is at the yarn centre. Accordingly the x and y coordinates of the original cross-section (the dashed line in Figure 6) can be defined by:

$$\begin{aligned} C(t)_x &= f(t) \quad 0 \le t \le 2\pi \\ C(t)_y &= q(t) \quad 0 \le t \le 2\pi \end{aligned} \quad (4)$$

Field Code Changed

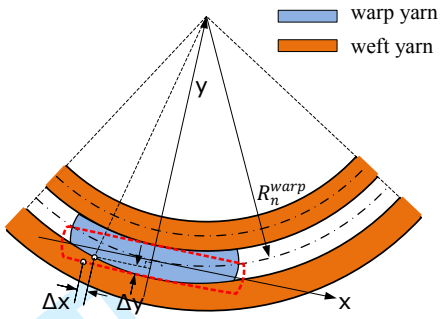

Figure 6. Schematic view of warp yarn cross-section bending

It is assumed that the bent shape is a result of a simple conformation of the major axis from the axis *x* to the arc in radius R_n^{Warp} (Eq.(1)). Thus, for each point on the upper half of the edge of a bent cross-section, the transformation can be achieved by adding (Δx, Δy) to the coordinates of corresponding points on the original cross-section, where Δx, Δy can be defined by:

$$\Delta x = (R_n^{warp} - H_{warp}/2)\sin(\frac{C(t)_x}{R_n^{warp} - H_{warp}/2}) - C(t)_x$$
$$\Delta y = (R_n^{warp} - H_{warp}/2)(1 - \cos(\frac{C(t)_x}{R_n^{warp} - H_{warp}/2})) \quad (5)$$

where H_{warp} is the height of the warp yarn. Similarly, for the point on the lower half of the edge of a bent cross-section, Δx, Δy are given by:

$$\Delta x = (R_n^{warp} + H_{warp}/2)\sin(\frac{C(t)_x}{R_n^{warp} + H_{warp}/2}) - C(t)_x$$
$$\Delta y = (R_n^{warp} + H_{warp}/2)(1 - \cos(\frac{C(t)_x}{R_n^{warp} + H_{warp}/2})) \quad (6)$$

Usually the value of $H_{warp}/2$ is quite small compared with R_n^{Warp}, thus the above equations can be simplified into one transformation for all the points on the cross-section:

$$\Delta x = R_n^{warp}\sin(\frac{C(t)_x}{R_n^{warp}}) - C(t)_x$$
$$\Delta y = R_n^{warp}(1 - \cos(\frac{C(t)_x}{R_n^{warp}})) \quad (7)$$

Field Code Changed

Field Code Changed

Field Code Changed

Weft yarn cross-section flattening

As shown in Figure 5 for half of a T-joint, each weft yarn is under a bending load. An idealized fibre distribution in the weft yarn would consist of parallel layers with concentric arcs whose arc lengths are dependent on each layer's radial position. For illustration, Figure 7 represents a multi-filament yarn by inner, middle and outer fibres/layers.

The model assumes that a fibre with high stiffness, such as carbon or glass fibre, has negligible axial deformation in a bent yarn. After folding a straight yarn (Figure 7(a)), it is clear that the assumed fibre arrangement in Figure 7(b) would lead to a fibre length difference which would not be realistic, in order to satisfy the boundary condition that a fibre bundle is undisturbed beyond the bending location. Meanwhile, Figure 7(c) shows another scenario where a fibre bundle with constant length complies with a 90^{o} bend resulting in fibre ends at a sheared angle, which contradicts the real boundary condition. Therefore, to maintain constant fibre length at a localised 90° bend, fibres tend to migrate and rearrange resulting in a flattened yarn cross-section as observed in Figure 4.

Taking the outermost layer of fibres in Figure 7(b) as a reference line for fibre movement, the rest of the fibres have to migrate to maintain their lengths. The positions of fibres except the reference ones in Figure 7(b) are considered as base positions for the movement. Hence the length differences between fibre on a specific fibre layer and fibre on the reference layer can be expressed as:

$$L_d = \frac{\pi}{2} d \qquad (8)$$

where d is the distance from a specific fibre layer within the yarn to the reference layer. In practice, d can be a series of discrete values depending on the fibre arrangement within the yarn.

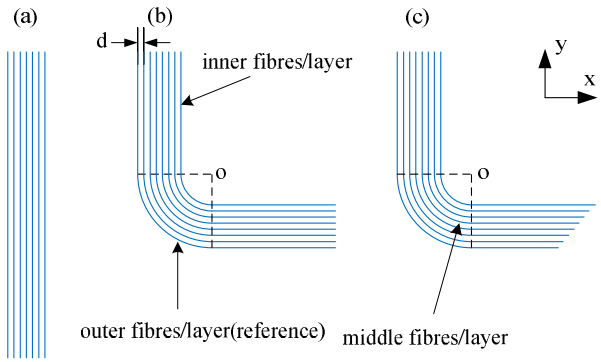

Figure 7. Idealized fibre arrangement in a 90° bent yarn

Field Code Changed

There are two possible mechanisms for a fibre to migrate that maintains fibre length at a bending corner. One mechanism is to move in the yarn height direction, referred to as in-plane migration (i.e. in the *x*-*y* plane shown in Figure 8). The other way is to move in the yarn width direction, referred to as out-of-plane migration (*z* direction in Figure 9). In-plane fibre migration will result in a reduction of yarn height while out-of-plane migration will increase the yarn width.

In-plane fibre migration

A reference fibre and a fibre on a neighbouring layer before and after migration are shown in Figure 8. The fibre loci in the bend can be approximated by circular paths as shown in Figure 3, thus in this model each single fibre path is described by one quadrant and two tangential straight lines, such as R_0, l_a^0 and l_b^0 in Figure 8 for example(where script *0* or *d* refers to reference or neighbouring layer). The positions of the two tangent straight lines are assumed to be fixed in migration based on the μCT observation that weft yarn height is almost unchanged in the region away from the bend. According to the length relation in two axial directions shown in Figure 8, the following expressions can be obtained:

$$l_a^0 + R_0 = l_a^d + R_d + d \quad (9)$$

Field Code Changed

$$l_b^0 + R_0 = l_b^d + R_d + d \quad (10)$$

Field Code Changed

where R_0 is the radius of curvature of the reference fibre that can be expressed by the sum of radius of curvature of yarn centreline and half of the flattened yarn height; R_d is radius of curvature of the fibre that is distance *d* away from the reference fibre.

If a proportion α of the above defined arc length difference as shown in Eq.(8) is compensated by in-plane fibre migration, the arc length difference between migrated and base fibres is $\pi d\alpha/2$. Thus the relation between the length of the reference fibre and a migrated fibre on a layer distance *d* away can be given as:

$$l_a^0 + \frac{\pi}{2}R_0 + l_b^0 = l_a^d + \frac{\pi}{2}R_d + l_b^d + L_d(1-\alpha) \quad (11)$$

Field Code Changed

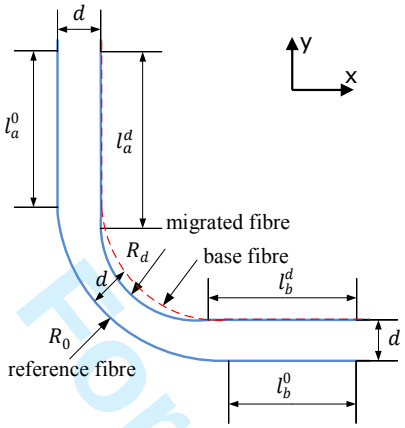

Figure 8. Schematic view of in-plane fibre migration

Hence, the in-plane path of a migrated fibre at distance *d* away from the reference fibre is described by:

$$R_d = R_0 - d - \frac{\pi\alpha d}{4-\pi}$$

$$l_a^d = l_a^0 + \frac{\pi\alpha d}{4-\pi}$$

$$l_b^d = l_b^0 + \frac{\pi\alpha d}{4-\pi} \quad (12)$$

Field Code Changed

Out-of-plane fibre migration

Since a proportion α of the defined fibre length difference is compensated by in-plane fibre rearrangement, the rest of the length difference, i.e. *(1-α)* of the whole length difference, has to be compensated by out-of-plane fibre migration to meet the assumption that the folding process would not increase the arc length of each fibre within a 90° bent yarn. In theory fibres can migrate in both directions across the yarn width.

In Figure 9, L_{ABCD} is the arc of a fibre which had in-plane but no out-of-plane migration so that its arc length is given by:

$$L_{ABCD} = \overline{AB} + \widehat{BC} + \overline{CD} = 2(l_0 - R_d) + \frac{\pi}{2}R_d \quad (13)$$

Field Code Changed

where l_0 is the length of yarn width transition, denoted by length between A(or D) and G, from where the yarn width starts to change.

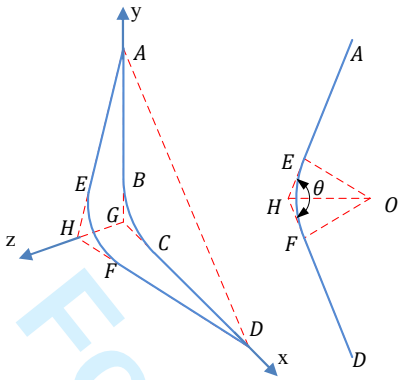

Figure 9. Schematic view of out-of-plane fibre migration

To calculate the arc length of a post-migration fibre L_{AEFD}, it is assumed that its radius of curvature is still the same as L_{ABCD}. $\overline{GH}$ denotes the distance that the fibre has migrated laterally, therefore in ΔADH we can have:

$$\sin^2\frac{\theta}{2} = \left(\frac{\overline{AD}/2}{\overline{AH}}\right)^2 \quad (14)$$

Field Code Changed

Also, in ΔAGH and ΔADG we can have:

$$\overline{AH}^2 = \overline{AG}^2 + \overline{GH}^2;\ \overline{AD}^2 = \overline{AG}^2 + \overline{GD}^2 \quad (15)$$

Field Code Changed

Hence, Eq.(14)~~(14)~~ is given by:

Formatted: Font:

$$\sin^2\frac{\theta}{2} = \frac{\frac{1}{2}l_0^2}{l_0^2 + w^2} \quad (16)$$

Field Code Changed

where for simplicity l_0 equals $\overline{AG}$ or $\overline{DG}$; w equals $\overline{GH}$.
From trigonometry we can say that:

$$\tan^2\frac{\theta}{2} = \frac{l_0^2}{l_0^2 + 2w^2} \quad (17)$$

Field Code Changed

Hence, in ΔEHO $\overline{EH}$ is given by:

$$\overline{EH} = \frac{\overline{EO}}{\tan\frac{\theta}{2}} = \frac{R_d}{\tan\frac{\theta}{2}} \quad (18)$$

Field Code Changed

The arc length of migrated fibre L_{AEFD} is:

$$L_{AEFD} = \overline{AE} + \widehat{EF} + \overline{FD}$$
$$= 2\left(\sqrt{l_0^2 + w^2} - \frac{R_d\sqrt{l_0^2 + 2w^2}}{l_0}\right) + R_d\left(\pi - 2\tan^{-1}\left(\frac{l_0^2}{l_0^2 + 2w^2}\right)\right) \quad (19)$$

Field Code Changed

Thus, the relation between fibre arc length differences caused by out-of-plane fibre migration can be represented by:

$$L_{AEFD} - L_{ABCD} = L_d(1 - \alpha) \quad (20)$$

Field Code Changed

Substituting Eq.(13)~~(13)~~ and Eq.(19)~~(19)~~ into Eq.(20)~~(20)~~, the displacement for out-of-plane migration w can be obtained for a fibre at a distance d away from the reference fibre.

Formatted: Font:

Formatted: Font:

Formatted: Font:

Yarn cross-section

The process of fibre migration resulting from bending is complex, as each single fibre may have a different value of α for its in-plane and out-of-plane migrations. Ideally, if all fibres on the same layer move with the same α and direction for out-of-plane migration, the cross-section of a weft yarn, assuming a square array for fibre packing, at Section A-A in Figure 2 would have a parallelogram shape as shown in Figure 10(b), where Figure 10(a) is the fibre arrangement before flattening with its left-hand layer as reference for in-plane migration (Figure 8). Since there are thousands of fibres in a single yarn, a large number of fibres presumably might migrate uniformly in the above way, i.e. without a change to their initial relative spatial sequence, as shown for the fibres represented by black dots in Figure 10(c) which remain in their ideal positions as in Figure 10(b). Meanwhile, a few fibres, not following the above ideal migration law, can penetrate into a position out of their own layers through more in-plane migration once out-of-plane migration of fibres on prior layers makes a space, as indicated by grey dots in Figure 10(c), which can cause a random serrated cross-section shape as observed in Figure 4. Additionally, a second possible cross-section shape is shown in Figure 10(d) if it is assumed fibres move with the same α but in both directions for out-of-plane migration. Hereafter the first large group of fibres following the pre-migration relative spatial sequence are named ideally migrated fibres, and the second small group are called randomly migrated fibres. Under this assumption, the values of α for the ideally migrated fibres are supposed to be identically denoted by $\bar{\alpha}$. Therefore the yarn height could be characterised by the distance between two corresponding fibres on the outermost layer(reference) and on the innermost layer respectively as shown in Figure 11.

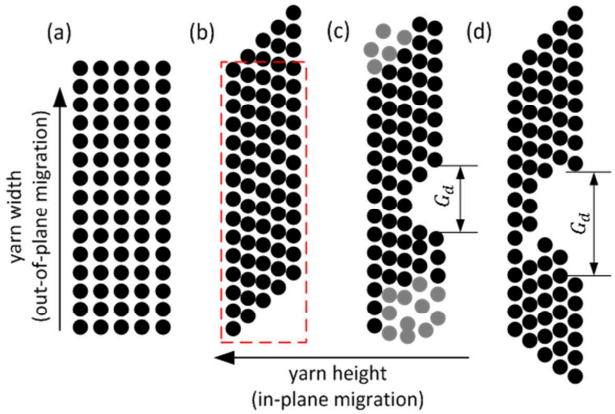

Figure 10. Schematic cross-section of fibre arrangement for a weft yarn showing fibre migration mechanisms: (a) pre-migration, square packing fibre arrangement; (b) post-migration, idealized migration; (c) and (d) post-migration, possible realistic migration accounting for serrated cross-section shape

If the flattened yarn height (at Section A-A in Figure 2) can be measured from a μCT scan, the value of $\bar{\alpha}$ for ideally migrated fibres on the innermost layer could be calculated by solving the following equation after substituting $R_{d_{max}}$ with Eq.(12)~~(12)~~:

$$H_{weft}^{fla} = R_0 - R_{d_{max}} - \sqrt{2}dx \quad (21)$$

where d_{max} is the maximum value of d which is the original yarn height; $(-dx, -dy)$ in Figure 11 is the position of the centre of curvature of a fibre on the innermost layer in the coordinate system of reference fibre with its centre of curvature as origin, which is given by:

$$dx = dy = R_0 - R_{d_{max}} - d_{max} \quad (22)$$

The yarn width is determined by the fibres that had out-of-plane migration. Irrespective of randomly migrated fibres and considering all fibres to be ideal ones migrating in the yarn width direction with an identical $\bar{\alpha}$, the relative migration displacement w could be obtained by solving a combination of Eq.(13)~~(13)~~, (19)~~(19)~~ and (20)~~(20)~~. In this case, if the yarn extension, defined as the area beyond its original cross-section (area of fibres outside of the dotted rectangle in Figure 10(b)), for the flattened yarn is full of ideally migrated fibres, the total fibre area for fibres in the yarn extension can be roughly estimated by:

$$Area_{ext} = \sum_{k=1}^{n_f} w_k d_f \quad (23)$$

Formatted: Font:
Field Code Changed
Field Code Changed
Formatted: Font:
Formatted: Font:
Formatted: Font:
Field Code Changed

where d_f is the fibre diameter and n_f is the number of total fibre layers along the yarn height direction before flattening; w_k is the displacement of out-of-plane migration for a fibre on layer k.

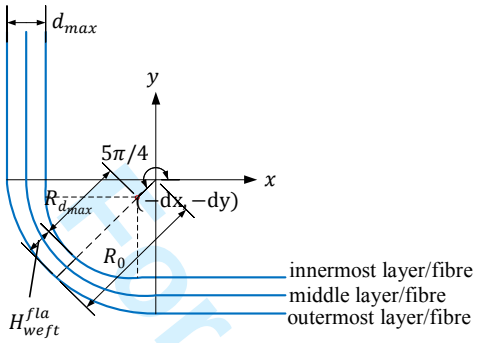

Figure 11. Yarn in-plane section view ($\bar{\alpha}$=0.4; d_{max}=0.35)

In reality, ideally migrated and randomly migrated fibres coexist in a bent yarn so that a flattened cross-section can be near to rectangular with the observed gap (Figure 4) rather than a parallelogram (Figure 10 (b)) if all fibres are considered ideally migrated fibres. Some of the fibres, namely randomly migrated fibres, in the yarn extension do not have to move that much in the yarn width direction because there is enough space ahead of them to accommodate in-plane migration in the yarn height direction, in the meantime the bending force will prioritise in-plane migration. Therefore a rectangular cross-section is likely to be formed, and a rough prediction of weft yarn width extension W_{weft}^{ext} in terms of constant fibre area in the yarn extension can be made by:

$$W_{weft}^{ext} = Area_{ext} / H_{weft}^{fla} \quad (24)$$

Field Code Changed

where the value of H_{weft}^{fla} should be known in advance.

However, it is not possible that different fibres on the same layer can move in both directions simultaneously for out-of-plane migration as shown in Figure 10(d), because the measured G_d is much smaller than double the value of maximum w_k as calculated in the following section. Hence the predicted flattened yarn width can be expressed as:

$$W_{weft}^{fla} = W_{weft} + W_{weft}^{ext} \quad (25)$$

Field Code Changed

where W_{weft} is the original weft yarn width. This model is capable to predict the change of yarn cross-section if H_{weft}^{fla} can be determined.

Validation

Three proposed models for warp yarn shifting, cross-section bending and weft yarn cross-section flattening were compared to experimental data from the standard orthogonal weave region of the preform as listed in Table 1.

Warp yarn shifting

The value of R_m is 2mm which equals the radius at the junction of the acrylic fixture contacting the preform. Based on Eq.(1)~~(1)~~, the radii of curvature of centrelines for warp cross-sections and weft yarns on different yarn layers can be obtained as listed in Table 2, which shows good agreement with the measured values.

The offset distance d_o for the preform is measured as 2.0mm and thus the relative angle shift of a warp yarn can be derived by Eq.(2). Furthermore, the displacement shift in adjacent layers can be determined by Eq.(3)~~(3)~~. Since the yarn shift is not significant for this preform, the angle shit measurements were only taken between yarns on layer 1 and yarns on other layers, whilst the displacement shift measurements were carried out between yarns on layer 2 and 3, as numbered in Figure 3. The warp yarns shift in a uniform manner but show a deviation along the yarn length direction. The measured shift values taken at different cross-sections along the length direction with standard deviations are shown in Table 3 in comparison with predicted values.

It is noticed that the measured angle shit between layer 1 and 3 is negative, which means the warp yarn on layer 3 has slid to the flange while folding. Also it is the same with displacement shit for yarns on layer 1 and 4 in the next warp stack.

Table 3. Warp yarn shift measured and predicted results (10 measurements)

	Angle shift S_θ (°)between			Displacement shift S_d (mm)
	layer 1 and 2	layer 1 and 3	layer 1 and 4	between layer 2 and 3
Measured value	2.96(±0.23)	-1.48(±0.17)	6.48(±0.25)	0.87(±0.13)
Predicted value	2.63	4.55	6.01	0.69

Warp yarn stack shift can be observed but the trend does not always agree closely with the model since binder yarns influence the movement of warp yarns as well as yarn sliding induced by the weaving process.

Formatted: Font:

Formatted: Font:

Warp yarn cross-section bending

A bent cross-section shape can be obtained by the transformation defined in Eq.(7) on the basis of an original parameterized cross-section description. Figure 12(a) is based on an elliptical cross-section and its radius of curvature of centreline is 3mm; Figure 12(b) is transformed from a super-ellipse (Eq.(26)) with m=0.4 where radius of curvature of centreline of bent yarn cross-section is 2.4mm.

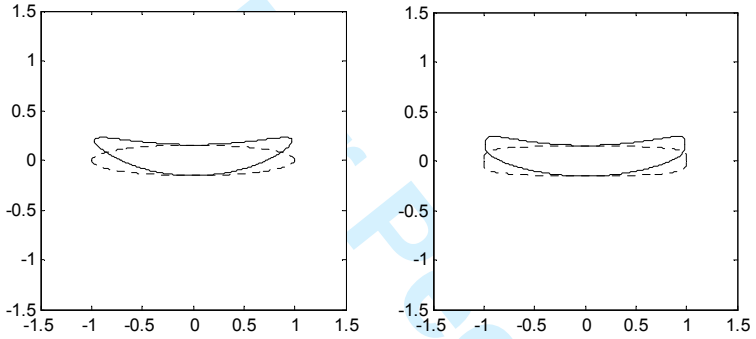

(a) elliptical cross-section (b) super-elliptical cross-section

Figure 12. Transformation of bent yarn cross-section shapes: dashed lines for original shapes and solid lines for bent shapes

It is observed that a real warp cross-section shape for this preform in the flat region can be better approximated with a super-ellipse than an ellipse, thus validation of warp yarn bending is based on the cross-section function for super-ellipse (m=0.4) with yarn height and width measured from the unbent region in the web, where Eq. (4) can be expressed as:

$$C(t)_x = \frac{W_{warp}}{2}\cos(t) \qquad 0 \le t \le 2\pi$$

$$C(t)_y = \begin{cases} \frac{H_{warp}}{2}\sin^m(t) & 0 \le t \le \pi \\ -\frac{H_{warp}}{2}(-\sin(t))^m & \pi \le t \le 2\pi \end{cases} \qquad (26)$$

Then the bent cross-sections for different radii of curvature can be plotted and compared with real yarns as shown in Figure 13. The modelled cross-section gives good agreement with realistic bent cross-section shapes.

Field Code Changed

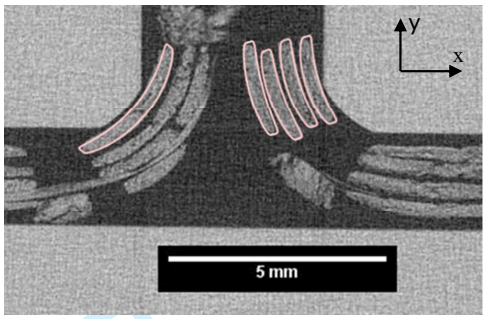

Figure 13. Model produced cross-section shapes in comparison with real yarns

Weft yarn cross-section flattening

Validation of cross-section flattening was carried out for yarns on three different layers in order to cover the full radius of curvature values which are the most essential parameters in yarn bending. The three layers selected are layer 1, 2 and 5 in section A-A of Figure 4. Weft yarn cross-section transition length l_0 is obtained from measurement for each layer, and radius of curvature of the reference fibre R_0 is derived based on calculated radius of curvature yarn centreline and flattened yarn height.

The total number of fibre layers along the yarn height direction before flattening n_f (Eq.(23)~~(23)~~) is estimated based on yarn dimensions before flattening and filament count as well as the assumption that the cross-section was a rectangular shape with square fibre packing. Based on the flattened yarn height, $\bar{\alpha}$ can be obtained by solving a combination of Eq.(12)~~(12)~~, (21) and (22). Then the displacement of fibre out-of-plane migration along the yarn height if all the fibres are ideally migrated ones can be obtained by solving a combination of Eq.(13)~~(13)~~, (19)~~(19)~~ and (20)~~(20)~~ as plotted in Figure 14. Yarn extension width can be calculated from Eq.(23) and (24), and all the parameters for the prediction model are listed in Table 4.

Formatted: Font:

Formatted: Font:

Formatted: Font:

Formatted: Font:

Formatted: Font:

Table 4. Parameters for the yarn flattening prediction model

	l_0 (mm) 10 measurements	R_0 (mm)	$\bar{\alpha}$ (-)	d_{max} (mm)	n_f (-)	W_{weft}^{ext} (mm)	W_{weft}^{fla} (mm)
Yarn on layer 1	4.54(±0.18)	2.32	0.132	0.35	50	1.22	2.93
Yarn on layer 2	4.86(±0.16)	2.77	0.062	0.32	44	1.15	3.15
Yarn on layer 5	6.31(±0.14)	4.09	0.062	0.32	44	1.46	3.46

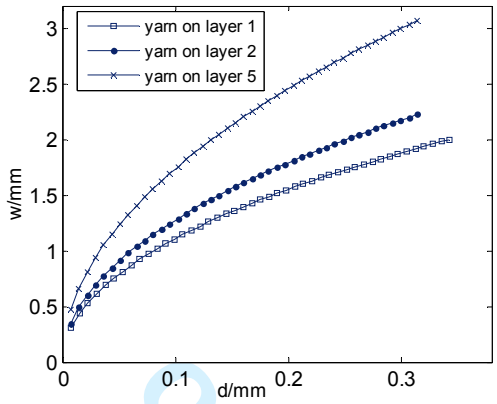

Figure 14. Relative displacement for fibre out-of-plane migration

Furthermore, the measured yarn width and predicted yarn width for the flattened weft yarns are compared in Figure 15 and reasonable agreement is observed.

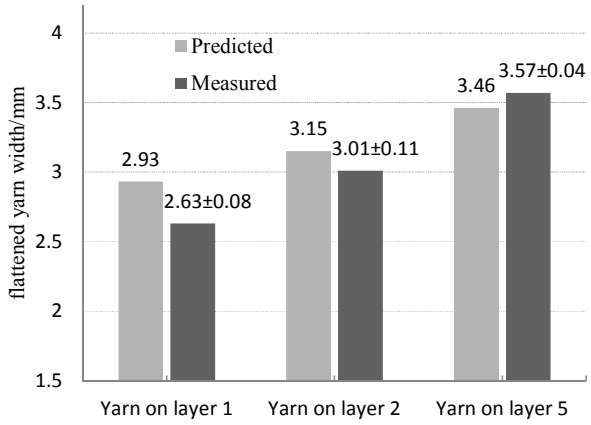

Figure 15. Comparison of measured and predicted yarn width for weft yarns

Although the prediction accuracy is good, the model is semi-empirical based on the input parameters of flattened yarn height and cross-section transition length. However it is interesting that all the flattened weft yarns with different radii of curvature have nearly the same height while the length over which cross-section transitions occur seems to increase linearly with radius of curvature in bending, both of which are merit further investigation.

Conclusions

To characterise the relationship between the fibre architecture and composite mechanical performance, a numerical simulation requires a realistic geometric model as input. In this study, three geometric features, yarn shifting, cross-section bending and flattening, caused by the bifurcation of a 3D flat woven preform for composite T-joints were identified by μCT analysis and approximated analytically. A simple model based on rigid body movement was used to approximate warp yarn shifting but the experimentally observed trend does not always agree closely with the model. The model would benefit from considering the influence of binder yarns on movement of warp yarns as well as yarn sliding induced by the weaving process but this would complicate the model significantly. Yarn cross-section bending was modelled by a transformation of the existing parameterized description of cross-section shape instead of proposing a new shape function, and good agreement was obtained when compared with μCT results. Lastly, weft yarn flattening was described in detail and a semi-empirical model was developed to predict the flattened yarn width and satisfactory agreement with experiments was observed. However, it is worthwhile to further study the preform compaction behaviour and form a fully predictive model for yarn flattening.

Declaration of Conflicting Interests

The authors declare that there is no conflict of interest.

Funding

This work was supported by the Engineering and Physical Sciences Research Council (EPSRC), United Kingdom [grant number: EP/IO33513/1], through the EPSRC Centre for Innovative Manufacturing in Composites.

References

1. Bilisik K. Multiaxis three-dimensional weaving for composites: A review. *Text Res J* 2012; 82: 725-743.

2. Cartié DDR, Dell'Anno G, Poulin E, et al. 3D reinforcement of stiffener-to-skin T-joints by Z-pinning and tufting. *Eng Fract Mech* 2006; 73: 2532-2540.

3. Koh TM, Feih S and Mouritz AP. Strengthening mechanics of thin and thick composite T-joints reinforced with z-pins. *Composites Part A* 2012; 43: 1308-1317.

4. Soden JA, Weissenbach G and Hill BJ. The design and fabrication of 3D multi-layer woven T-section reinforcements. *Composites Part A* 1999; 30: 213-220.

5. Chiu CH and Cheng CC. Weaving Method of 3D Woven Preforms for Advanced Composite Materials. *Text Res J* 2003; 73: 37-41.

6. Fazeli M, Hübner M, Lehmann T, et al. Development of seamless woven node element structures for application in integral constructions. *Text Res J* 2015; 86: 1220-1227.

7. Fazeli M, Kern M, Hoffmann G, et al. Development of three-dimensional profiled woven fabrics on narrow fabric looms. *Text Res J* 2015; 86: 1328-1340.

8. Khokar N. 3D-weaving: Theory and practice. *J Text Inst* 2001; 92: 193-207.

9. Amirul I. 3D woven structures and an overview of manufacturing techniques. In: *4th World Conference on 3D Fabrics and Their Applications*, Aachen, Germany, 2012.

10. Chen X, Taylor LW and Tsai LJ. An overview on fabrication of three-dimensional woven textile preforms for composites. *Text Res J* 2011; 81: 932-944.

11. Thomson RS, Falzon PJ, Nicolaidis A, et al. The bending properties of integrally woven and unidirectional prepreg T-sections. *Compos Struct* 1999; 47: 781-787.

12. Mouritz AP and Cox BN. A mechanistic interpretation of the comparative in-plane mechanical properties of 3D woven, stitched and pinned composites. *Composites Part A* 2010; 41: 709-728.

13. Endruweit A, McGregor P, Long AC, et al. Influence of the fabric architecture on the variations in experimentally determined in-plane permeability values. *Compos Sci Technol* 2006; 66: 1778-1792.

14. Skordos AA and Sutcliffe MPF. Stochastic simulation of woven composites forming. *Compos Sci Technol* 2008; 68: 283-296.

15. Fast T, Scott AE, Bale HA, et al. Topological and Euclidean metrics reveal spatially nonuniform structure in the entanglement of stochastic fiber bundles. *J Mater Sci* 2015; 50: 2370-2398.

16. Yan S, Long A and Zeng X. Experimental assessment and numerical analysis of 3D woven composite T-joints under tensile loading. In: *Proceedings of the 20th International Conference on Composite Materials (ICCM 20)*, Copenhagen, Denmark, 2015.

17. Desplentere F, Lomov SV, Woerdeman DL, et al. Micro-CT characterization of variability in 3D textile architecture. *Compos Sci Technol* 2005; 65: 1920-1930.

18. Karahan M, Lomov SV, Bogdanovich AE, et al. Internal geometry evaluation of non-crimp 3D orthogonal woven carbon fabric composite. *Composites Part A* 2010; 41: 1301-1311.

19. Sherburn M. *Geometric and Mechanical Modelling of Textiles*. PhD Thesis, University of Nottingham, UK, 2007.

20. Lin H, Brown LP and Long AC. Modelling and Simulating Textile Structures Using TexGen. *Adv Mat Res* 2011; 331: 44-47.

21. Stig F and Hallstrom S. Spatial modelling of 3D-woven textiles. *Compos Struct* 2012; 94: 1495-1502.

22. Lomov SV, Gusakov AV, Huysmans G, et al. Textile geometry preprocessor for meso-mechanical models of woven composites. *Compos Sci Technol* 2000; 60: 2083-2095.

23. Mahadik Y and Hallett SR. Finite element modelling of tow geometry in 3D woven fabrics. *Composites Part A* 2010; 41: 1192-1200.

24. Zhou G, Sun X and Wang Y. Multi-chain digital element analysis in textile mechanics. *Compos Sci Technol* 2004; 64: 239-244.

25. Lomov SV and Verpoest I. Compression of woven reinforcements: A mathematical model. *J Reinf Plast Compos* 2000; 19: 1329-1350.

26. Chen ZR, Ye L and Kruckenberg T. A micromechanical compaction model for woven fabric preforms. Part I: Single layer. *Compos Sci Technol* 2006; 66: 3254-3262.

27. Chen ZR and Ye L. A micromechanical compaction model for woven fabric preforms. Part II: Multilayer. *Compos Sci Technol* 2006; 66: 3263-3272.

28. Cornelissen B and Akkerman R. Analysis of yarn bending behaviour. In: *Proceedings of the 17th International Conference on Composite Materials (ICCM 17)*, Edinburgh, Scotland, 2009.

Reviewer: 1

Comments to the Author

I have accepted the changes in the article. After answered on reviewers paper is more understanding. I recommend the paper for publication.

Response to reviewer 1:

This reviewer accepted the paper without any further questions.

Reviewer: 2

Comments to the Author
The revised Paper does not provide satisfactory answers to any of the questions and points raised earlier. It is therefore rejected.

The authors, when dealing with 'woven materials', 'interlacing', 'weaves' etc., ought to possess at least some basic understanding of the weaving subject, especially when submitting to the Textile Research Journal. Their confusion is clearly reflected in the opening statement under Point 5: "These deformations would not happen if it was an interlaced material." Obviously, by accepting that the material they are dealing with is is not interlaced, i.e. it is not a woven material, it is unclear what exactly their work then concerns.

In view of the above, the explanations and changes provided in respect to the points raised earlier have no relevance. For this work to scientifically advance the textiles field it ought to comply with established technicalities of textiles, particularly woven materials.

Response to reviewer 2:

Reviewer 2 did not raised any specific technical comments on this paper, but keeps claiming the subject material in this paper, i.e. 3D orthogonal woven preform, is not a type of woven materials based on the reviewer 2's knowledge, as the reviewer pointed out that only plain, twill, satin or any variants, which have interlaced warp or weft yarns, are considered as woven materials in his/her previous comment.

The authors had added a brief introduction to 3D woven materials (P2 line 34-41, highlighted) and a description on how binder yarns are interlacing with straight warp and weft yarns in a 3D orthogonal weave (P5 line 19-23 (highlighted), & Fig.2-b) in the previous manuscript, after they realised not all Textile Research Journal readers are in the textile composite field, along with several relevant papers on 3D woven materials as references for this study. Unfortunately, review 2 did not comment any of the above revisions. However, most of the cited references on 3D woven materials were publications of Textile Research Journal (ref.1,5,6,7,10), which contradicts the reviewer 2's viewpoint on the "established technicalities" of woven materials.

Reviewer: 3

Comments to the Author
This is an excellent, well written, timely paper, contacting detailed information on the models, real geometric structure of the preform - will be very useful for on-going and perspective research worldwide

Response to reviewer 3:

This reviewer accepted the paper without any further questions.

Reviewer: 4

Comments to the Author
This paper addresses a simple model of local geometry deformation in T-joints of 3D woven preforms. Since the local geometric anomaly can affect the mechanical property of 3D composites, its quantification and further FEM analysis would be an important part of reliable application of composite structures. Several researchers have pointed out the geometry deformation, but the modelling work was very rare. This work will contribute to the research of 3D textile composites because it is useful not only in the bifurcation of T-joints but also in the right-angle curved structure. Many questions raised by reviewers were clearly answered by authors, and were reflected in the revised manuscript.

I have a few additional questions in Page 5:
(1) In line 45, “4mm thickness in the web and 2mm in the flange” is not correct because the scale bar in Fig. 2 (c) indicates 5~6mm in the web and 3mm in the flange. Please, check the length of the scale bar.
(2) In line 47, I think the warp yarns in the flange (and curved region?), not in the noodle region, are in twice the filament count. The noodle region as indicated in the arrow has no fibers. The arrow indication of ‘2x12k’ on the web in Fig.2 (c) should be removed because it locates on the web. Is the filament count 24k in the curved region?
(3) In line 53~55, the last sentence would be duplicated if the above mention in question (2) is correct.

Response to reviewer 4:

(1) the length of scale bar in Fig.2 (c) was corrected.

(2) "in the noodle region" was changed to "at the junction (curved region)" on line 42, Page 5. To avoid misunderstanding, “in the noodle region” was changed to “at the junction” throughout this paper. Change was made to Fig.2 (c) by removing the arrow indication.

(3) Repetition was clarified after changes made according to question (2). Therefore, line 42-43 describes the 24k warp yarns used at the left-hand side of the junction and line 47-49 describes the 24k warp yarns in the flange.